



HAL
open science

Recent studies of docking and molecular dynamics simulation for liquid-phase enantioseparations

Paola Peluso, Alessandro Dessì, Roberto Dallochio, Victor Mamane, Sergio Cossu

► **To cite this version:**

Paola Peluso, Alessandro Dessì, Roberto Dallochio, Victor Mamane, Sergio Cossu. Recent studies of docking and molecular dynamics simulation for liquid-phase enantioseparations. *Electrophoresis*, In press, 2019, 40, pp.1881-1896. 10.1002/elps.201800493 . hal-02106485

HAL Id: hal-02106485

<https://hal.science/hal-02106485v1>

Submitted on 15 May 2020

HAL is a multi-disciplinary open access archive for the deposit and dissemination of scientific research documents, whether they are published or not. The documents may come from teaching and research institutions in France or abroad, or from public or private research centers.

L'archive ouverte pluridisciplinaire **HAL**, est destinée au dépôt et à la diffusion de documents scientifiques de niveau recherche, publiés ou non, émanant des établissements d'enseignement et de recherche français ou étrangers, des laboratoires publics ou privés.

1 **Recent studies of docking and molecular dynamics simulation**
2 **for liquid-phase enantioseparations**

3 **Paola Peluso,^{1,*} Alessandro Dessì,¹ Roberto Dallochio,¹ Victor Mamane,² and Sergio Cossu³**

4 ¹Istituto di Chimica Biomolecolare ICB CNR – Sede Secondaria di Sassari, Traversa La Crucca 3,
5 Regione Balduina, 07100 Li Punti - Sassari, Italy

6 ²Institut de Chimie de Strasbourg, UMR 7177, Equipe LASYROC, 1 rue Blaise Pascal, BP 296 R8,
7 67008 Strasbourg Cedex, France

8 ³Dipartimento di Scienze Molecolari e Nanosistemi DSMN, Università Ca' Foscari Venezia, Via
9 Torino 155, 30172 Mestre Venezia, Italy

10
11 ***Correspondence:** Dr. Paola Peluso, Istituto di Chimica Biomolecolare ICB CNR – Sede Secondaria
12 di Sassari, Traversa La Crucca 3, Regione Balduina, I-07100 Li Punti - Sassari, Italy

13 **E-mail:** paola.peluso@cnr.it

14
15 **Abbreviations:** **ADMPC**, amylose *tris*(3,5-dimethylphenylcarbamate); **AMBER**, assisted model
16 building with energy refinement; **CCMPC**, cellulose *tris*(3-chloro-4-methylphenylcarbamate); **CCPC**,
17 cellulose *tris*(3-chlorophenylcarbamate); **CDCPC**, cellulose *tris*(3,5-dichlorophenylcarbamate);
18 **CDMPC**, cellulose *tris*(3,5-dimethylphenylcarbamate); **CF**, cyclofructan; **CHARMM**, chemistry at
19 Harvard macromolecular mechanics; **CM**, carboxymethyl; **CMB**, cellulose *tris*(4-
20 methylphenylbenzoate); **CSP**, chiral stationary phase; **DC**, dielectric constant; **EEO**, enantiomer elution
21 order; **EMO**, enantiomer migration order; **ESH**, explicit σ -hole; **GOLD**, genetic optimisation for ligand
22 docking; **HB**, hydrogen bond; **HBA**, hydrogen bond acceptor; **HBD**, hydrogen bond donor; **ITC**,
23 isothermal titration calorimetry; **LGA**, Lamarckian genetic algorithm; **MD**, molecular dynamics;
24 **MeOH**, methanol; **MM**, molecular mechanics; **MP**, mobile phase; **NP**, normal phase; **PABA**, *p*-
25 aminobenzoic acid; **PEP**, positive extra point; **PO**, polar organic; **RMSD**, root mean square deviation;
26 **SFC**, supercritical fluid chromatography.

27
28 **Keywords:** Chiral stationary phase / Docking / Liquid-phase enantioseparation / Molecular dynamics /
29 Molecular recognition

30 **Abstract**

31 Liquid-phase enantioseparations have been fruitfully applied in several fields of science. Various
32 applications along with technical and theoretical advancements contributed to increase significantly the
33 knowledge in this area. Nowadays, chromatographic techniques, in particular HPLC on chiral stationary
34 phase, are considered as mature technologies. In the last thirty years, CE has been also recognized as one
35 of the most versatile technique for analytical scale separation of enantiomers. Despite the huge number
36 of papers published in these fields, understanding mechanistic details of the stereoselective interaction
37 between selector and selectand is still an open issue, in particular for high-molecular weight chiral
38 selectors like polysaccharide derivatives. With the ever growing improvement of computer facilities,
39 hardware and software, computational techniques have become a basic tool in enantioseparation science.
40 In this field, molecular docking and dynamics simulations proved to be extremely adaptable to model
41 and visualize at molecular level the spatial proximity of interacting molecules in order to predict
42 retention, selectivity, enantiomer elution order, and profile noncovalent interactions patterns underlying
43 the recognition process. On this basis, topics and trends in using docking and molecular dynamics as
44 theoretical complement of experimental LC and CE chiral separations are described herein. The basic
45 concepts of these computational strategies and seminal studies performed over time are presented, with a
46 specific focus on literature published between 2015 and November 2018. A systematic compilation of
47 all published literature has not been attempted.

48

49

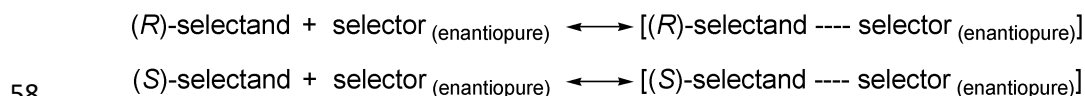
50

51

52

53 1 Introduction

54 In keeping with chiral recognition mechanisms occurring in biochemical environment,
55 enantioseparation science is based on the concept that a chiral enantiopure molecule (selector) can
56 recognize the enantiomer pair of a chiral analyte (selectand) through noncovalent interactions which
57 underlie the distinction process [1] (Scheme 1).



59 **Scheme 1.** Equations describing the concept of enantioseparation by means of the reversible and dynamic formation of
60 diastereoisomers between *R/S* enantiomer pair of selectand and selector.

61 In LC on chiral stationary phase (CSP), a dynamic process, occurring by means of adsorption-
62 desorption steps between CSP and mobile phase (MP), enables the transformation of two enantiomers
63 into transient diastereomeric complexes, which are characterized by different chemo-physical properties
64 and different ΔG values, $\Delta\Delta G_{R,S}^{\circ}$ being related to the enantioseparation factor (α) through the equation
65 $\Delta\Delta G_{R,S}^{\circ} = -RT \ln \alpha$. Enantiorecognition occurs on the basis of the same principle when chiral selector is
66 introduced in the chromatographic system as an additive to MP, but this technique is rarely used in LC.

67 Differently, in CE the chiral selector is usually added to the BGE as part of the MP and, therefore,
68 selector-selectand complexes are mobile. As a consequence, in this case two principles govern
69 enantioseparations [2,3]: i) the chromatographic enantioselective recognition, occurring at molecular
70 level, between selector and selectand, and ii) the electrophoretic enantioselective separation which is due
71 to different mobility of the diastereomeric complexes.

72 In the last decades, both LC and CE techniques have been successfully employed in
73 enantioseparation science [2,4-9]. Despite the huge number of papers published in these fields, the
74 understanding of the stereoselective interaction process is still an open issue. Indeed, multiple
75 noncovalent interactions along with other effects can promote retention and enantioseparation [6]: i)
76 strong long-range interactions involved in the primary non-stereoselective binding, ii) non-

77 stereoselective adsorption of analytes to the solid support, iii) short-range directional noncovalent
78 interactions [1], underlying the stereoselective binding, which are governed by complementarity of
79 functional groups, like hydrogen bond (HB), π - π interactions, dipole-dipole stacking and the emergent
80 halogen bond [10,11], iv) steric factors deriving from the spatial arrangement of selector binding site, v)
81 conformational changes of selector induced by selectand binding, vi) hydrophobic effects, and vii)
82 solvation effects. This high level of complexity concerns in particular high-molecular weight selectors
83 such as polysaccharide derivatives.

84 Chromatographic studies and retention models, spectroscopy methods based on FT-IR and NMR, X-
85 ray crystallography analysis, and computational methods, which include both chemoinformatics and
86 molecular modelling, have been developed for several years with the aim of gaining information on
87 binding strength and structure of selector-selectand complexes, and type of involved noncovalent
88 interactions [1,2,6]. In particular, computational tools contributed to overcome some disadvantages of
89 using other techniques like low solubility of certain selectors and limited reliability of solid state models
90 to describe complexes in solution, observed for spectroscopy and X-ray crystallography, respectively.

91 Molecular mechanics (MM) methods are widely applied in structure refinement of large molecular
92 systems for which the quantum mechanics (QM) approach is, in general, time-consuming from a
93 computational point of view. MM uses potential-energy functions to model molecules, which consist of
94 spherical atoms connected by springs representing bonds [12,13]. An important aspect of modelling
95 enantioselection concerns the concept of molecular potential energy surface which determines shape and
96 dynamic features of the related molecule. In this regard, two main questions have to be tackled, namely
97 where to locate selectand, in or around the selector [14], and how many selector-selectand complexes
98 must be computed (and sample among all the possible reciprocal orientations) to make the calculation
99 really representative of the experimental system [1]. As response to the questions, *docking* and
100 *molecular dynamics* (MD) are exploited to reduce the number of sampling on the potential energy
101 surface and define initial and equilibrium mutual positioning of selector and selectand. Thus, both

102 methods are often used as theoretical complement of experimental liquid-phase enantioseparations with
103 the general purpose to visualize the complex associations and provide a molecular-level understanding
104 of structure and dynamics of the CSP, retention mechanisms of analytes, interactions of analytes and
105 CSP, and solvation effects at the CSP interface [15].

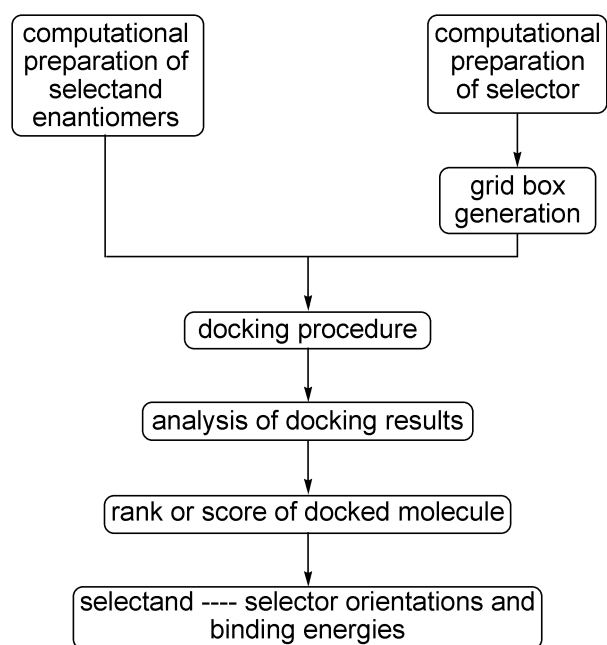
106 On this basis, recent representative applications of both docking and MD simulations in LC and CE
107 enantioseparations are presented herein, covering years 2015-2018 (November). Nevertheless, previous
108 seminal and basic studies in the field are also cited for further information. In this regard, some
109 applications of molecular modelling can be found in some excellent reviews concerning chiral
110 recognition mechanisms [1,2,6,16,17] published in the period 2010-2017. In particular, molecular
111 simulation studies in reversed-phase liquid chromatography [15] and computational studies to rationalize
112 chromatographic EEO [18] have been reviewed in the last years as specific topics in the field. Moreover,
113 it is worth highlighting that seminal papers on atomistic model of enantioselective binding and MD
114 theory in chromatography have been published by Lipkowitz [14,19,20] and Felinger [21], respectively.

115 Although theoretical details on computational methods are beyond the scope of this review, in the
116 next two paragraphs a brief description of aims and working basis of both docking and MD is provided.

117 **2 Molecular docking and dynamics in liquid-phase enantioseparations**

118 Molecular docking is generally used to simulate the interaction between the enantiomer pairs and the
119 active site of the selector in order to predict both energy and geometry of selector-selectand binding. A
120 docking process consists of two general steps, namely conformational search through various
121 algorithms, and scoring or ranking of the docked conformations (selector-selectand mutual orientations)
122 (Fig. 1) [22]. The majority of the studies reported in enantioseparation science have been carried out
123 with AutoDock [23] and AutoDockTools as graphical interface [24]. AutoDock employs Lamarckian
124 Genetic Algorithm (LGA) [23] to identify binding conformations of the selectand, as a flexible ligand, to
125 the selector. Genetic algorithm methods describe the three-dimensional arrangement of the molecules
126 involved in the docking by using geometrical (state) variables which, in this specific case, are selector-

127 selectand distance, the orientation of selectand with respect to the selector, and the torsional degrees of
128 freedom (number of rotatable bonds) of the selectand enantiomers [25]. The program uses a simplified
129 form of AMBER (Assisted Model Building with Energy Refinement) forcefield (see § 3) for the energy
130 calculations, and the free energy of binding is calculated by computing van der Waals and Coulombic
131 energy contributions between all atoms of selector and selectand through an empirical functional form
132 [26].



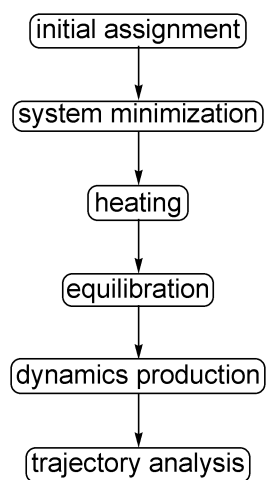
133

134 **Figure 1.** Flow diagram of a general docking protocol.

135 In the preliminary preparation step to docking, three-dimensional grid boxes are created by using
136 AutoGrid, which is a module in AutoDock generating a simplified representation of the selector.
137 Usually, for application in enantioseparation science, the grid box is set to around $80 \times 80 \times 80 \text{ \AA}$ with
138 0.375 \AA spacing. In the computational space profiled by the grid box, each atom type of the chiral
139 analyte is positioned and its interaction energy with each atom of the selector will be computed and
140 assigned to a grid point. All grid points collected for a particular atom-type constitute a map, and during
141 docking the maps are used for extracting interaction energies of the enantiomers with the selector. At the
142 end of docking calculations, several conformers of the enantiomers are obtained and clustered in several

143 sets. The results are given in terms of the mean binding energy of the clusters or the mean energy of the
144 most populated cluster, and their consistency with the experimental EEO is a basic requirement to
145 develop a reliable predictive model.

146 Introduced in chromatography by Giddings and Eyring in the mid of the last century [27], MD is a
147 simulation that shows how molecules move, vibrate, diffuse, and interact over time [28]. This approach
148 is based on classical mechanical equations of motion related to the enantioseparations system consisting
149 of interacting particles [15]. Several software have been made available, and nowadays commonly used
150 programs for MD simulations include AMBER [29] and CHARMM (Chemistry at HARvard
151 Macromolecular Mechanics) [30], among others. The MD protocol normally consists of six phases:
152 initial assignment, system minimization, heating, cooling, equilibration, and trajectory production (Fig.
153 2) [31].



154

155 **Figure 2.** Flow diagram of a general MD protocol.

156 On the basis of this sequence, the molecular system is free to run for a period of time and the process
157 is iterated for thousands of steps in order to bring the system to an equilibrium state, saving all the
158 information about the atomic positions, velocities, and other variables as a function of time. The set of
159 data emerging from the MD experiment is called trajectory that profiles positions and velocities of the
160 chiral partners in the system and their variation with time. All the equilibrium and dynamic properties of
161 the system can be calculated from trajectory data set. Interestingly, the root mean square deviation

162 (RMSD) of all atoms in a molecule can be plotted against time to summarize the degree of fluctuation
163 for the entire structure.

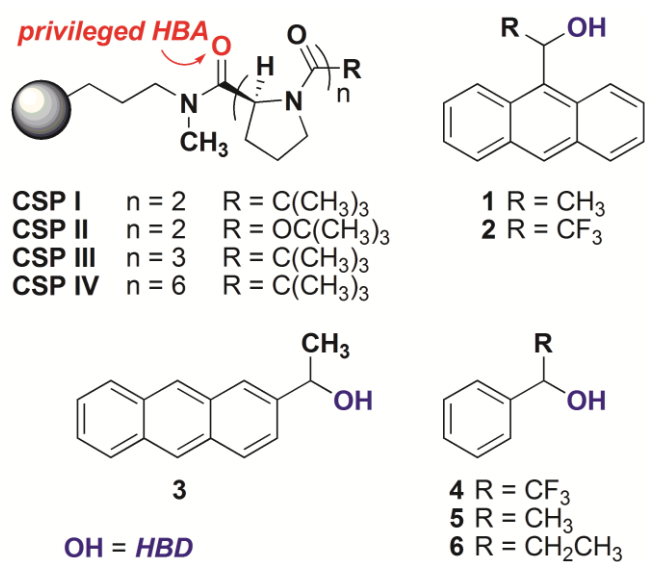
164 Taking into account that solvent can strongly influence the energy of different complex orientations,
165 in MD simulations solvent can be parametrized by treating it explicitly or implicitly [32]. Explicit-
166 solvent methods introduce solvent molecules by computing interactions between all pairs of solute and
167 solvent atoms, whereas implicit-solvent methods speed up simulations by approximating the discrete
168 solvent as a continuum, thus drastically reducing the number of particles in the system. Moreover, in
169 docking as well as in MDs the proper dielectric constant (DC) value can be used to define the screening
170 effect of solvent on noncovalent interactions, with values ranging from 1 (vacuum) to 80 (water) [26].

171 Docking calculations and MD simulations can be combined [33,34] to model selectand enantiomers
172 into selectors. First, docking techniques are used to explore a vast conformational space in a short time
173 and scan the possible diastereomeric orientations with the aim of reducing sampling. Then, more
174 accurate MD simulations can be applied when few complexes have been selected. Indeed, a problem of
175 docking concerns the poor flexibility of the selector, which is not permitted to adjust its conformation
176 upon selectand binding, whereas MD treats simulations in a flexible way. However, MD simulations are
177 time-consuming and the length of time that can be saved during a trajectory sampling (usually from ten
178 to hundreds of nanoseconds) is limited by the computer performances and time available. This question
179 can be particularly crucial in modelling large systems. Consequently, in these cases, focused
180 approximations or specific computational techniques are usually applied on a case by case basis. In the
181 next paragraphs, recent applications of docking and MD simulations are discussed on the basis of
182 selector type.

183 **3 Donor-acceptor chiral selectors**

184 Donor-acceptor chiral selectors (also called brush-type or Pirkle-type selectors) contain small
185 molecules which are anchored in a silica matrix [35]. These CSPs are able to exert electrostatic
186 interactions based on complementarity like HB, π - π interactions and dipole-dipole stacking. In the

187 previous decade, some interesting procedures were developed to model enantiomer distinction on Pirkle-
 188 type CSPs. Cann and co-workers published a series of relevant papers over time concerning the
 189 application of MD simulations to explore the solvation at the Whelk-O1 interface [36-38] and the
 190 docking modes of different selectands [37]. Interestingly, Gasparri and co-workers developed a
 191 general scheme based on a systematic and automatic “quasi-flexible” docking approach for studying
 192 stereoselective recognition mechanisms, validating it on a leucine-containing Pirkle-type selector
 193 [39,40]. Following previous theoretical studies involving proline-based selector interfaces [41,42],
 194 recently Cann and Ashtari employed MD simulations (35-40 ns of simulation time) to model the
 195 enantioseparation of six closely related aromatic analytes **1-6** on four polyproline-based CSPs **I-IV** (Fig.
 196 3) [43].



197
 198 **Figure 3.** Structures of Pirkle-type polyproline selectors and aromatic alcohols as selectands in MD simulations [43].

199 In this study, 48 MD simulations were undertaken, considering each solvent (2) + selector (4) +
 200 analyte (6) combination, on a modelled surface consisting of 16 polyprolines, 64 silanol groups, 48
 201 trimethylsilyl end-caps and 128 fixed Si atoms. The theoretical study was performed by considering the
 202 effect of two different MPs, namely *n*-hexane/2-propanol, as a nonpolar mixture, and water/methanol, as
 203 polar MP, on chiral recognition. In addition, due to focused structure variations in the series of CSPs, the
 204 selected chiral selectors allowed an analysis of the impact of oligomer length and terminal group on

205 selectivity. On this basis, simulations gave the following information: i) the occurrence of an alternative
 206 recognition mechanism in water/methanol compared to the NP elution conditions because of a different
 207 HB solvent pattern and a diverse conformational preference of the proline chains; ii) crowding at the
 208 interface increases for **CSP IV**, affecting the arrangement of analyte docking into the surface; iii) the
 209 carbonyl oxygens close to the Si layer appeared preferentially involved in chiral recognition as HBA; iv)
 210 HB is the main interaction governing recognition and selectivity coupled with steric hindrance effects at
 211 the chiral surface. When possible, the calculated selectivities were compared with the experimental
 212 values, finding a good overall agreement (Table 1).

Table 1. Predicted selectivity factors ($\alpha_{\text{predicted}}$), under NP elution conditions (*n*-hexane/2-propanol 70:30), derived from MD simulations [43], and available experimental selectivity values ($\alpha_{\text{experimental}}$) for the enantioseparation of **1-6** on CSPs **I** and **IV**

Analyte	$\alpha_{\text{predicted}} (\alpha_{\text{experimental}})$	
	CSP I	CSP IV
1	1.40 ± 0.13 (1.61)	1.92 ± 0.08 (2.60)
2	1.46 ± 0.10 (1.51)	1.77 ± 0.09 (2.08)
3	1.21 ± 0.11 (1.10)	1.09 ± 0.14 (1.00)
4	1.03 ± 0.16 (1.06)	1.00 ± 0.15 (1.10)
5	1.13 ± 0.15 (1.10)	1.08 ± 0.16 (1.00)
6	1.07 (1.10)	1.12 ± 0.16 (1.00)

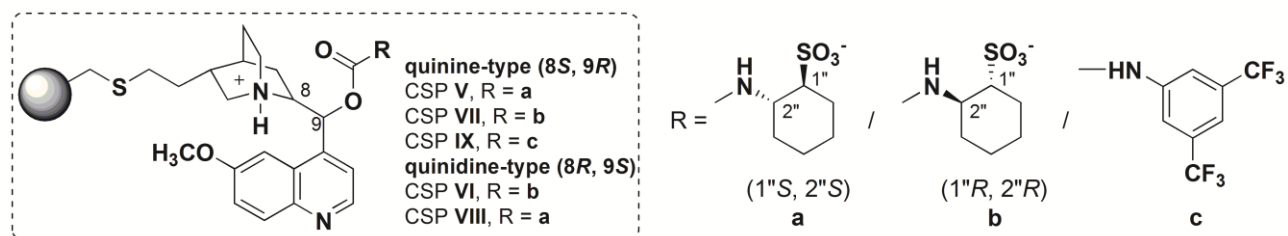
213 Topal and co-workers performed both docking and MD simulation (175 ps of simulation time) with
 214 AutoDock and AMBER programs, respectively, to investigate chiral recognition mechanism governing
 215 the enantioseparation of mandelic acid and 2-phenyl propionic acid on a Pirkle-type CSP synthesized by
 216 the authors, finding a good correlation between theoretical and experimental results [44].

217 **4 *Cinchona* alkaloid-based selectors**

218 In the last years, CSPs based on *Cinchona* alkaloids, in particular their zwitterionic (ZWIX) version,
 219 have been widely used for enantioseparation of chiral acids, amino acids and peptides [45]. These chiral
 220 ion-exchange CSPs, which have pioneered by Lindner [46], interact with charged analytes via HB or π - π
 221 interactions as other donor-acceptor chiral supports. Nevertheless, long-range ionic interactions between
 222 charged selector and selectands also occur. In this field, Natalini, Sardella and co-workers developed a
 223 MD simulation protocol (Desmond Molecular Dynamic System 4.0/4.4/5.2 program, 300 ns of

224 simulation time) [47,48], which recently has been extensively applied, in collaboration with other
 225 groups, to investigate chiral recognition mechanisms and rationalize experimental EEO observed with
 226 different *Cinchona* alkaloids-based CSPs under RP elution [49] and polar organic (PO) [50-52] elution
 227 conditions (Table 2).

Table 2. Recent MD simulation studies involving *Cinchona* alkaloid-based CSPs V-IX [49-52]



CSP	Analyte	MD environment and main results	References
V, VI	<p><i>N</i>^t-Boc-<i>N</i>^d-(hydroorotylyl)-4-aminophenylalanine [Boc-Aph(Hor)-OH]⁹ stereoisomers (4)</p>	<p>custom solvent: ACN/MeOH/water 49.7:49.7:0.6^{a)}</p> <p><i>main results</i></p> <ul style="list-style-type: none"> - confirmation of EEO_{exp}: D,D < D,L < L,D < L,L - active role of achiral element of the CSPs and solvent - observation of HBs between the sulphonic acid group of CSP V and two or three amidic groups of the hydroorotic fragment 	2015 Sardella [49] (diastereo- and enantioseparation)
V-VIII	<p>(+) and (-) <i>trans</i>-paroxetine enantiomers</p>	<p>custom solvent: MeOH/THF 80:20^{a)}</p> <p><i>main results</i></p> <ul style="list-style-type: none"> - interaction pattern between paroxetine and CSPs - confirmation of EEO_{exp} of paroxetine on CSPs VII and VIII - limited EEO prediction power of the model for CSPs V and VI due to its intrinsic inability to consider entropic contributions 	2016 Ilisz [50] 2018 Carotti [51]
IX	<p>cyclopropyl dafachronic acid derivative stereoisomers (4)</p>	<p>custom solvent: ACN</p> <p><i>main results</i></p> <ul style="list-style-type: none"> - confirmation of EEO_{exp}: <i>cisoid</i> forms < <i>transoid</i> forms, with (24S,25R) < (24R,25S) < (24S,25S) < (24R,25R) 	2018 Sardella [52]

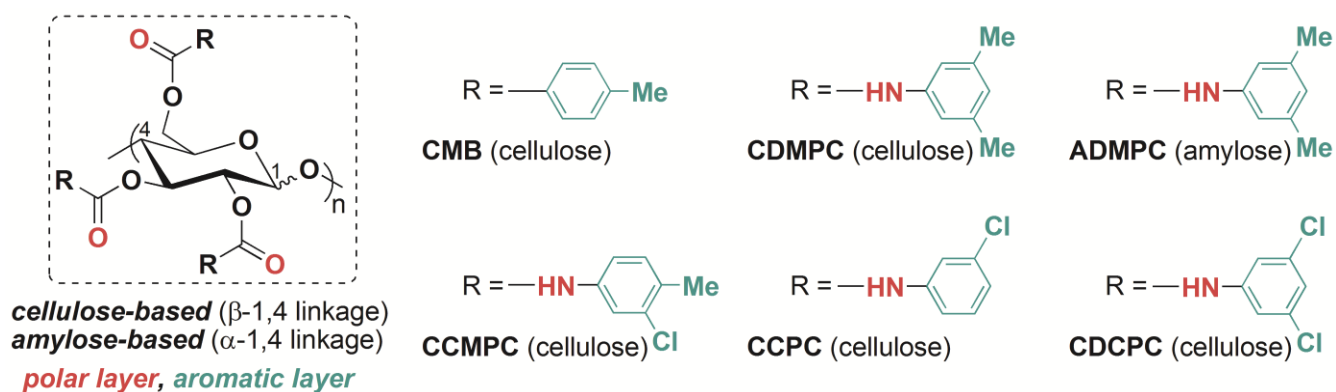
229 a) Boc, t-butyloxycarbonyl; MeOH, methanol

230 The protocol is based on the calculation of three energy descriptors: the interaction energy between
 231 the selector unity and the whole discrimination system (named INTER), the interactions energy between
 232 selector and selectand (INTER_SA) and the conformational energy of selectand (SELF), relative to its
 233 minimum energy derived by the collected MD snapshots. Once energy values are calculated, the matrix
 234 is submitted to two *k-means clustering* runs as a method for cluster analysis to identify families of
 235 interactions and the suitable number of clusters which are evaluated and correlated to the experimental

236 outcomes [53]. For a realistic reproduction of the CSP, in these studies a surface containing 4
 237 mercaptopropyl-functionalized silanols, 8/16 free silanols and 45 Si atom (keeping frozen during MD)
 238 was considered for each selector unit. It is worth noting that, in this case, selector being anchored in
 239 achiral support, achiral sub-structural elements are also considered on the modelled surface because non-
 240 enantioselective adsorption sites have been found to contribute to retention behaviour.

241 5 Polysaccharide derivatives

242 Currently, polysaccharide-based CSPs are the most used for LC enantioseparations. These selectors
 243 are characterized by a modular polymeric system where molecular, conformational, and supramolecular
 244 chirality cooperate to determine the separation outcome [1]. Their structure consists of a glucosyl
 245 backbone (cellulose or amylose linkage), derivatized by carbamate or benzoate functionalities with an
 246 internal polar layer, and an aromatic layer, functioning as modulator of the electronic properties of the
 247 polar layer (Fig. 4). Firstly introduced by Okamoto and co-workers [54], the versatility of
 248 polysaccharide derivatives as chiral selectors was improved by Chankvetadze and co-workers by
 249 introducing halogen substituents on the phenyl rings [4].



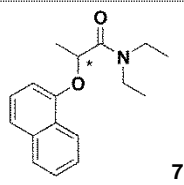
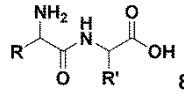
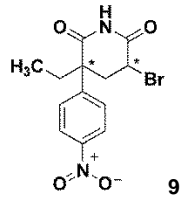
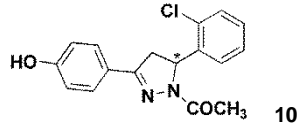
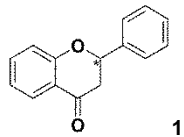
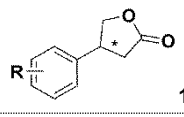
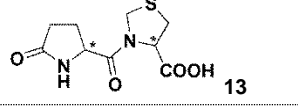
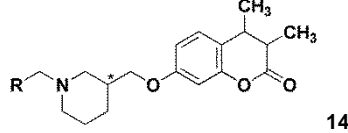
252 Starting for the '90s, seminal studies dealing with modelling of polysaccharide-based selectors and
 253 related enantioseparations have been published by the groups of Okamoto [55-57], Franses [58-60], and
 254 Grinberg [61,62]. In addition, further interesting modelling studies were performed on polysaccharide-
 255 derivatives and published in the last years [63-67]. In Figure 4, the structures of some polysaccharide

256 selectors modelled over time are reported. All these studies contributed to understand some aspects of
257 the chiral recognition: i) the chromatographic behaviour can depend on the polymer backbone as well as
258 on the type of side chain; ii) attractive interactions play an important role in the recognition as well as
259 the steric fit of the analyte inside the chiral cavity, where polar carbamate groups are considered as
260 important chiral adsorbing sites. Nevertheless, understanding the recognition mechanism at molecular
261 level is still demanding due to the intrinsic complexity of these selectors.

262 In Table 3, a summary of some representative docking and MD studies published in the period 2015-
263 2018 is reported [68-78]. Firstly, in modelling polysaccharides, an important issue concerns the
264 preparation of a built polymer which is representative of the 'real' polysaccharide derivative. On the
265 basis of the studies of Okamoto's group, cellulose *tris*(3,5-dimethylphenylcarbamate) (**CDMPC**) and
266 amylose *tris*(3,5-dimethylphenylcarbamate) (**ADMPC**) have been characterized by a left-handed (3/2)
267 and 4/3 helix, respectively. Usually, oligomeric fragments composed of 12 monomers are used, despite
268 sometimes studies involving shorter oligomers have been reported probably to reduce computational
269 time. In this regard, recently Liu and co-workers reported a molecular docking studies by using trimer
270 fragments to model CDMPC, ADMPC and cellulose *tris*(3-chloro-4-methylphenylcarbamate)
271 (**CCMPC**) and the enantiomers of napropamide **7** as analytes [68]. On this basis, the study partly
272 explained the variations of experimental EEOs observed with the three CSPs under supercritical fluid
273 chromatography (SFC) conditions (CO₂/modifier = alcohol or ACN). Indeed, variations of the HB
274 features between enantiomers of **7** and each CSP were considered to justify the EEO of *S-R* and *R-S*
275 observed on amylose and cellulose CSPs, respectively. In other recent studies, fragment of 5-6
276 monomers have been considered. Ali and co-workers studied both diastereo- and enantioseparation of a
277 large series of dipeptides **8** on ADMPC by using molecular docking [69,70]. Later, the same authors also
278 modelled by docking the recognition of the four stereoisomer of 5-bromo-3-ethyl-3-(4-
279 nitrophenyl)piperidine-2,6-dione **9** on ADMPC [71].

280

281 **Table 3.** Recent docking and MD simulation studies involving polysaccharide-based selectors [68-78]

CSP ^{a)}	Analyte	Modelling technique, software, medium	References
ADMPC, CDMPC, CCMPC	 7	Docking , Molegro Virtual Docker (MolegroApS, DK-800 Aarhus C, Denmark), vacuum	2018 Liu [68]
ADMPC	 8	Docking , AutoDock 4.2 (Scripps Research Institute, USA), vacuum	2015 Ali [69,70]
ADMPC	 9	Docking , AutoDock 4.2, vacuum	2016 Ali [71]
CDCPC	Enantiomers of eightazole antifungals	Docking , AutoDock 4.2, vacuum	2018 Li [72]
CCPC	Enantiomers of eight anticholinergic drugs	Docking , AutoDock 4.2, vacuum	2018 Guo [73]
CMB	 10	Molecular dynamic , Material Studio (Accelrys USA), medium is accounted for by the use of dielectric constants corresponding to vacuum and seven eluents	2016 Huang [74]
ADMPC	 11	Molecular dynamic , AMBER 14 (University of California, San Francisco, USA), Explicit-solvent (MeOH and <i>n</i> -heptane/2-propanol)	2017 Murad [75]
ADMPC	 12	Docking , AutoDock 4.2, MP is accounted for by the use of dielectric constants corresponding to four eluents	2017 Collina, Abate [76]
ADMPC	 13	Docking , GOLD, vacuum	2015 Shen [77]
ADMPC	 14	Docking , AutoDock 4.2, vacuum	2018 Altomare [78]

282 a) **ADMPC**, amylose *tris*(3,5-dimethylphenylcarbamate); **CCMPC** cellulose *tris*(3-chloro-4-methylphenylcarbamate); **CCPC** cellulose *tris*(3-
283 chlorophenylcarbamate); **CDCPC** cellulose *tris*(3,5-dichlorophenylcarbamate); **CDMPC** cellulose *tris*(3,5-dimethylphenylcarbamate); **CMB**
284 cellulose *tris*(4-methylphenylbenzoate).

285 This year, the first modelling by docking of chloro-substituted polysaccharide selectors have been
286 reported. Indeed, enantioselection of eightazole antifungals (Table 4) on the chlorinated cellulose
287 *tris*(3,5-dichlorophenylcarbamate) (**CDCMC**) has been modelled by Li and co-workers by using
288 molecular docking [72]. The variation of the binding energies (average energy of the best cluster with
289 the lowest docking energy) of the complexes formed by *R*- and *S*-enantiomers was in agreement with the

290 observed enantioselectivity under NP elution conditions (Table 4). Guo and co-workers reported a
 291 docking study, modelling cellulose *tris*(3-chlorophenylcarbamate) (**CCPC**) as selector and the
 292 enantiomers of eight anticholinergic drugs (atropine sulfate, phenylcyonate, dipivefrine hydrochloride,
 293 tropicamide, homatropine methylbromide, oxybutynin, scopolamine hydrobromide, benzhexol
 294 hydrochloride) [73].

Table 4. Correlation between the variation of the binding energies (average energy of the best cluster with the lowest docking energy) of the complexes formed by *R*- and *S*-enantiomers and selectivity factors on **CDCPC**^{a)} under NP elution

Analyte	$ \Delta\Delta E$ [kcal/mol] ^{b)}	α
Butoconazole	0.71	1.95
Ornidazole	0.55	1.46
Sulconazole	0.47	1.29
Enilconazole	0.38	1.27
Isoconazole	0.35	1.25
Econazole	0.33	1.24
Ketoconazole	0.26	1.21
Futrimazole	0.11	1.06

295 a) **CDCPC**, cellulose *tris*(3,5-dichlorophenylcarbamate)

296 b) $|\Delta\Delta E$ [kcal/mol] = $|\Delta E_R - \Delta E_S|$

297 The composition of the MP can have a very important effect on chiral recognition, therefore the
 298 effect of solvent should be considered in theoretical computational studies. Huang and co-workers
 299 modelled the enantioselection of a chiral pyrazole derivative **10** on cellulose *tris*(4-methylbenzoate)
 300 (**CMB**) by means of MDs (100ps of simulation time) [74]. In the study, a 12-monomer fragment was
 301 built to model CMB, with the terminal monomers replaced by methyl groups, and seven mixtures were
 302 used as custom solvents. DC values were set by the authors to represent the experimental conditions as
 303 follows: *n*-hexane/ethanol (70/30) (DC = 9.06), *n*-hexane/2-propanol (60/40) (DC = 8.58), pure ethanol
 304 (DC = 25.80) and pure 2-propanol (DC = 18.62). In addition, three reference solvent conditions, vacuum
 305 (DC = 1), pure *n*-hexane (1.89) and water (81.00) were also considered in order to explore the solvent
 306 effect systematically. The computational experiments showed that the solvent effect has an important
 307 influence on selector-selectand binding energies. Consequently, in polar solvents (DC \geq 8.58) the *S*-
 308 enantiomer...CSP complex appeared more stable than the *R*-enantiomer...CSP complex, according to

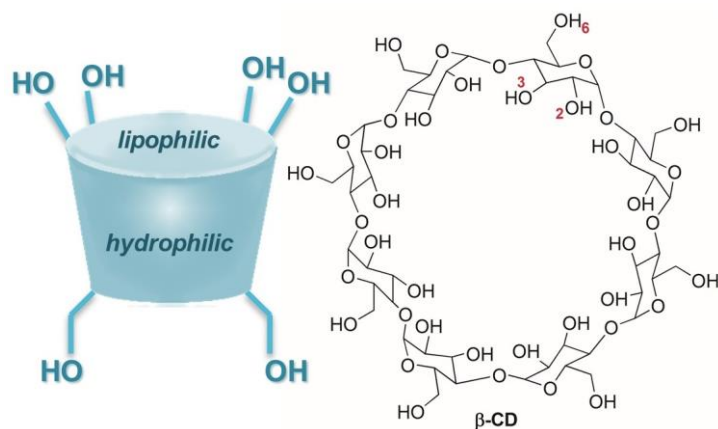
309 the experimental EEO of *R-S* reported for **10** by using PO solvent or NP with an alcohol content $\geq 30\%$.
310 Murad and coworkers used quantum mechanics (QM)/MM and MD simulations to model the
311 enantiomers of flavanone **11** on a 12-mer ADMPC (100 ns of simulation time) [75]. It is worth noting
312 that the hybrid QM/MM approach is not uncommon in this field because it combines the accuracy of
313 QM and speed of MM, allowing for the study of large molecules in solution. In this study, custom
314 solvents were introduced explicitly corresponding to MeOH 100% and heptane/2-propanol as
315 experimental eluents. Significantly, the simulations showed that the lifetime of HBs formed between
316 ADMPC and flavanone enantiomers are able to reproduce the EEO observed in the experiments
317 performed under PO and NP conditions. Abbate, Collina and co-workers described a series of molecular
318 docking experiments which were performed to justify the constant *S-R* EEO observed for all
319 enantiomeric pairs of four 3-aryl-substituted- γ -butyrolactones **12** on the ADMPC under NP and PO
320 elution conditions [76]. In this study, the MP composition was simulated by using DC values
321 corresponding to the experimental MPs. The mean docking energy proved to be consistent with the
322 chromatographic results and, for each enantiomeric pair, the higher calculated binding energy
323 corresponded to the first eluted (*S*)-enantiomer.

324 In principle, molecular docking can be performed in vacuum without modelling MP effect. In this
325 case, despite the fact that the variations of energy predicted by docking in vacuum could be different
326 compared to experimental results in solution, a good agreement can be also found. In this regard, Shen
327 and co-workers performed a comparative docking by using ADMPC and cyclodextrins (CDs) as
328 selectors and the enantiomers of pidotimod **13** as analytes. The difference of HBs, van der Waals, and
329 internal torsional tension energy between the enantiomers and CSPs were found to be the leading causes
330 of chiral recognition [77]. Altomare and coworkers modelled by docking the enantioseparation of three
331 coumarin derivatives **14** on a 12-mer ADMPC [78]. Interestingly, with the aim of achieving a plausible
332 low energy conformation, the authors subjected the ADMPC fragment to a short MD, assembling the

333 solvated model in an orthorhombic box filled with methanol molecules to mimic the MP (experimental
334 MP = MeOH/ACN).

335 6 Cyclodextrins

336 CDs are cyclic oligosaccharides formed by D-glucose units with α -1,4 linkages. These molecules are
337 characterized by a hollow toroid-shape, lipophilic inside and hydrophilic outside, where secondary 2-
338 and 3-hydroxyl groups are located at the wider rim, while primary 6-hydroxyl groups at the narrower
339 rim. Due to the possibility to modify chemically the hydroxyl groups, a large number of CD derivatives
340 are commercially available and immobilized to solid supports.



341
342 **Figure 5.** General scheme of CD hollow toroid-shape and structure of β -CD.

343 Despite the fact that ‘external’ complexes between CD derivatives and guest molecules have been
344 observed [79], the main complexation mode occurs via inclusion between an apolar part of the guest
345 molecule by hydrophobic interactions in the cavity, and polar interactions at the polar rim of the CD
346 [80]. Several noncovalent interactions underlie recognition processes like HBs, π - π and hydrophobic
347 interactions, dipole-dipole stacking, van der Waals and dispersion forces. On one hand, the fact that CDs
348 can be studied in solution allowed NMR to give a great contribution to understand their recognition
349 mechanism [81]. On the other hand the complexity of the possible recognition pattern which govern
350 inclusion, or external contacts, make molecular modelling a versatile tool also in this case.

351 Current trends in molecular modelling applied to the study of CDs have been recently reviewed [82]
352 with a specific focus on drug delivery matrixes and intelligent nanodevices such as CD-based molecular
353 motors. Moreover, in the last years Alvira performed a deep investigation on MD simulation approaches
354 to model amino acid enantiodiscrimination by using α -, β -, γ -CDs and a series of CD derivatives [83-
355 85]. Recently, Wang and co-workers modelled the enantioseparation of flavonone with β -CDs by MDs,
356 introducing the mixture MeOH/water 1:1 (RPLC conditions) as custom solvent [86]. Starting from a
357 different approach, López-Nicolás and co-workers modelled the contacts between methyl jasmonate
358 stereoisomers and methyl- β -CD by molecular docking, as theoretical complement of the experimental
359 enantioseparation performed by adding the selector to the MP, under RPLC conditions [87].

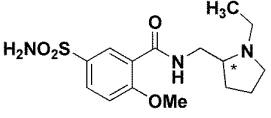
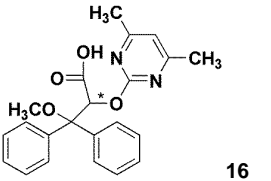
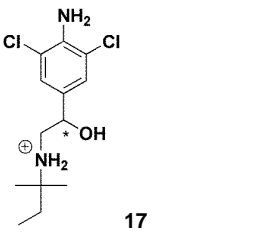
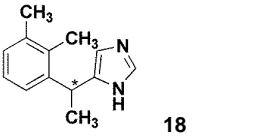
360 Due to some features like availability, low toxicity ad UV absorbance along with good solubility,
361 CDs have been largely applied as chiral selector in CE. Several studies concerning docking of CE
362 enantio recognition have been published in the last years [88-92]. In this regard, it is worth mentioning
363 that despite the fact that the prerequisite for separation of enantiomers is their enantioselective
364 interaction with a chiral selector, the EEO in CE does not necessarily correlate with the enantioselective
365 recognition, as it occurs in LC on CSP, because of the additional contribution of the electrophoretic
366 enantioseparation mechanism [2]. Moreover, as argued by Chankvetadze, CE is one of the most
367 sensitive tools for detecting very weak enantioselective noncovalent interactions because of the very
368 high separation efficiency, and energy difference between the diastereomeric complexes at the level of
369 few kJ/mol is sufficient for observing baseline separation of enantiomers. Nevertheless, this advantage
370 implicates that a reliable evaluation of such small energy differences by means of molecular modelling
371 requires the selection of the proper force field, charge state of selector and selectand, and proper
372 parametrization to account for solvent effect [2].

373 Using CDs as chiral selector in CE allows chiral recognition mechanisms to be studied in solution by
374 spectroscopic methods and separation techniques under similar conditions [2,81]. Recently, interesting

375 investigations of the complexation between CDs and enantiomers have been published, which are
376 performed by means of a multidisciplinary approach based on the use of CE, NMR and molecular
377 simulations (Table 5). You and co-workers performed the enantioseparation of four chiral drugs (2-
378 amino-1-phenylethanol, 1-(4-methoxyphenyl)-2-(methylamine)ethanol, salbutamol sulfate, sotalol
379 hydrochloride) by CE using both β -CD and carboxymethyl- β -cyclodextrin (CM- β -CD) that exhibited
380 the best separation efficiency [93]. In this study, isothermal titration calorimetry (ITC), NMR and
381 molecular docking were used to gain information about recognition mechanism. On this basis, it was
382 found that hydrophobic interactions, electrostatic interactions and HBs underlie the enantioselection
383 induced by the CM- β -CD. Orlandini, Furlanetto and co-workers developed a method for the
384 enantioseparation of sulpiride (**15**) enantiomers by CE with the addition of two types of CDs to the
385 BGE, namely the negatively charged sulfate- β -CD sodium salt and a neutral CD [80]. A
386 multidisciplinary approach based on both NMR and MD was used to investigate recognition mechanism.
387 MDs was performed with 3 ns of production time, in implicit solvent. On one hand, MD simulation
388 suggested, in agreement with CE experiments, a relationship between the gain in potential energy and
389 migration time. On the other hand, NMR showed the inclusion of the benzene sulphonamide moiety of
390 the analyte inside the hydrophobic cavity of the CDs. Very recently, the same author studied the
391 separation mechanism involved in CD-MEKC analysis of ambrisentan (**16**) enantiomers by means of the
392 combined CE/NMR/MD approach. The study provided information on the aggregates, inclusion
393 complexes and noncovalent interactions underlying the separation system [94]. Salgado and co-workers
394 used again NMR spectroscopy and MD (100 ns of production time) to investigate structure and energy
395 of the binding complexes between the enantiomers of clenpenterol **17** and two CDs, namely β -CDs and
396 heptakis(2,3-di-*O*-acetyl)- β -cyclodextrin (HAD- β -CD) [95]. The study showed that the inclusion mode
397 of **17** is dependent on CD structure and that intermolecular HBs are mediated by bridging water

398 molecules. Moreover, computed interaction energies proved to account for both enantioseparation and
 399 enantiomer migration order (EMO) reversal observed by changing β -CD to HAD- β -CD.

Table 5. Recent combined molecular modelling – NMR – CE investigations by using CDs as selectors [3,80,93-95]

CD ^{a)}	Analyte	Modelling technique, software, medium	References
β -CD CM- β -CD	2-amino-1-phenylethanol, 1-(4-methoxyphenyl)-2-(methylamine)ethanol, salbutamol sulfate, sotalol hydrochloride	Docking , AutoDock 4.2 (Scripps Research Institute, USA), vacuum	2015 You [93]
sulfate- β -CD sodium salt + neutral CD	 15	Molecular dynamics , AMBER (University of California, San Francisco, USA), implicit solvent	2015 Orlandini, Furlanetto [80]
γ -CD	 16	Molecular dynamics , AMBER, implicit solvent	2017 Orlandini, Furlanetto [94]
β -CD HAD- β -CD	 17	Molecular dynamics , AMBER, water box	2017 Salgado [95]
β -CD γ -CD HS- β -CD	 18	Molecular dynamics , AMBER, water box	2018 Scriba [3]

400 a) CM- β -CD, carboxymethyl- β -cyclodextrin; HAD- β -CD, heptakis(2,3-di-O-acetyl)- β -cyclodextrin; HS- β -CD, heptakis(6-O-sulfo)- β -CD.

401 Later, Scriba and coworkers investigated the influence on EMO of medetomidine (**18**) of both cavity
 402 size and substitution pattern of CDs used as selectors in CE environment [3]. Also, in this case, both
 403 NMR and MD simulations (100 ns simulation time) contribute to rationalize the binding mechanism,
 404 showing that for β -CD and γ -CD the phenyl moiety of medetomidine enter the cavity from the wider
 405 secondary rim of the CDs, while the protonated imidazole ring points toward the bulk solvent. In the
 406 complex with heptakis(6-O-sulfo)- β -CD (HS- β -CD), the protonated imidazolium moiety appears to be
 407 positioned inside the CD cavity interacting with the sulfate groups in position 6 of the glucose monomer.

408

409

410 **7 Miscellaneous selectors**

411 Cyclofructans (CFs), which have been introduced in separation sciences by Armstrong and co-
412 workers [96], are cyclic oligosaccharides composed of β -2,1 linked D-fructofuranose units. Showing an
413 opposite pattern compared to CDs, CFs have internal HB interactions and do not present hydrophobic
414 cavities. By using the simple *p*-aminobenzoic acid (PABA), Armstrong, Sun and co-workers [97]
415 demonstrated a pH driven complexation between CF6 (containing 6 fructose units) and PABA by using
416 a combined MD-NMR approach.

417 Among macrocyclic glycopeptides, the most important from an analytical perspective are
418 vancomycin, ristocetin A, teicoplanin and teicoplanin aglycone. The selector structure consists of
419 interconnected amino acid-based macrocycles, each macrocycle containing two aromatic rings. These
420 glycopeptides form a C-shaped basket, several interactions underlying recognition mechanisms like
421 HBs, π - π , dipole-dipole, ion-dipole, ionic and hydrophobic interactions [6]. Pinto, Fernandez and co-
422 workers modelled the contacts between thirty-one chiral xanthonic analytes and four macrocyclic
423 glycopeptides by docking [98]. The theoretical study showed that each glycopeptide featured different
424 patterns. Ali and co-workers modelled the enantioseparation of four quinolones on teicoplanin by
425 molecular docking, and HBs and π - π interactions were found to be the major forces for chiral
426 recognition [99].

427 Recently MD simulations were also exploited to study contact between enantiomers and molecularly
428 imprinted polymers [100], single wall carbon nanotubes [101], and chiral molecular micelles [102,103].
429 Moreover, docking was also used to model enantiodiscrimination events involving chiral ionic liquids,
430 as MP additives [104].

431 **8 Molecular dynamics simulations of σ -hole-driven enantioseparations**

432 In the last years, our groups investigated the factors governing HPLC enantioseparation of
433 atropisomeric halogenated 4,4'-bipyridines on polysaccharide-based CSPs [8,105-107]. Following these

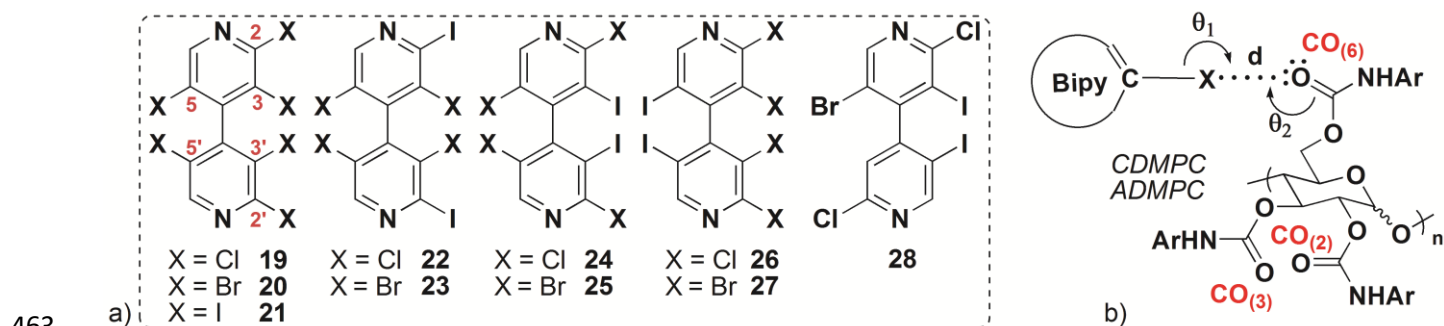
434 studies, we have demonstrated the contribution of halogen (XB) and chalcogen (ChB) bonds for the
435 enantio recognition of analytes on CDMPC [11,12,108-111].

436 XBs and ChBs are noncovalent interactions belonging to the family of σ -hole bonds which occur
437 between the electrophilic region (σ -hole) of the halogen or chalcogen atom (σ -hole donor) attached to
438 one molecule and the nucleophilic region of the interacting partner (σ -hole acceptor) [112]. Applications
439 involving both XB and ChB have rapidly grown in the last years and important advancements appeared
440 in supramolecular chemistry, biology and catalysis [113,114].

441 The electrophilic nature of halogens and chalcogens is due to the anisotropic distribution of the
442 electron density around these atoms [115]. Computational techniques have an essential role in
443 investigating this family of interactions, but conventional molecular mechanics (MM) force fields fail to
444 describe the XB because they did not account for the anisotropic distribution of the electron density.
445 Therefore, several MM approaches describing σ -hole in halogens were proposed in the last years [116].
446 Early 2010's, three groups have almost simultaneously shown that the σ -hole can be represented as a
447 positively charged dummy-atom. Ibrahim modelled the σ -hole as a massless point charge, called
448 positive extra point (PEP), placed on top of the halogen atoms and the optimal position of the PEP was
449 determined to be equal to the atomic radius of the halogen atom [117,118]. Sironi and co-workers
450 proposed almost exactly the same model where the pseudo-atom has a nonzero mass [119,120].
451 Introduced by Hobza and co-workers, the molecular mechanical explicit σ -hole (ESH) was constructed
452 as a massless point charge and the ESH parameters were fixed in terms of ESH-halogen distance and
453 units of the positive charge [121,122]. This approach of adding a partial positive charge in the region of
454 the σ -hole along the C-X axis was successfully implemented in the AMBER force fields package,
455 allowing significant improvement of the geometries and interaction energies for halogen-bonded
456 complexes. It has been later applied by Jorgensen and co-workers to enhance the OPLS-AA force field
457 for the description of halogens [123] and sulfur charge anisotropy [124]. The improved AMBER

458 program was successfully employed by different groups for MD studies in biological [125] and
 459 supramolecular systems [126,127]. Recently, XBs were also parametrized in CHARMM [128] and
 460 GROMOS [129] force fields.

461 On this basis, recently we used the ESH concept to model XB in CDMPC- and ADMPC-
 462 halobipyridine complexes by MD simulations (10 ns of simulation time) [109,110] (Fig. 6).

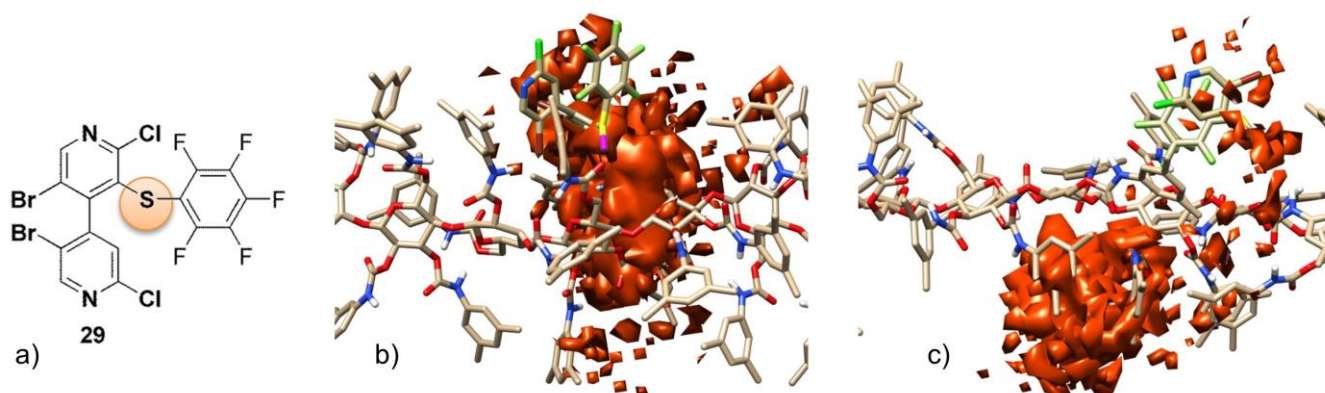


464 **Figure 6.** Structures of polyhalo-4,4'-bipyridines **19-28** used in MD studies and geometrical parameters (d , θ_1 , θ_2) of the
 465 XB complex between halogenated 4,4'-bipyridines and polysaccharide-based CSPs.

466 In all these studies, a massless dummy atom connected to I, Cl and Br was introduced manually, by
 467 using distance and charge values as described by Hobza and co-workers [122]. The parameters used for
 468 Cl, Br, I were 1.0, 1.3, 1.6 Å, and 0.1, 0.2, 0.3 units of positive charge for the extra point (EP),
 469 respectively. In order to keep the total charge of the molecule unchanged, an equivalent negative charge
 470 was manually added to each halogen atom. On the other hand, molecular models of 9-mer CDMPC and
 471 ADMPC were constructed in order to investigate on the binding sites functioning as σ -hole acceptors.
 472 The geometrical parameters analysed were i) the distance (d) between halogens and XBA centres, ii) the
 473 angle (θ_1) formed by aromatic carbon, halogen, and oxygen atom ($C-X\cdots O$, reference value 180°), and
 474 iii) the angle (θ_2) formed by halogens, carbonyl oxygen and carbonyl carbon ($X\cdots O=C$, reference value
 475 120°) (Fig. 6b). In particular, any distance shorter than the sum of the van der Waals radii of oxygen and
 476 halogen may be considered as an implication of XB. It is worth noting that, in general, θ_1 angles ranging
 477 from 160° to 180° are considered acceptable to decide if the interaction corresponds to a XB.

478 The potential contacts occurring in the course of the MDs on 4,4'-bipyridine **19-28** were examined.
479 Indeed, taking into account the dynamic feature of the enantioseparation event, the distances between
480 each of the six halogens as donor recognition sites and 14 points (N, O, H) located on each monomers of
481 the 9-mers CDMPC and ADMPC were statistically analyzed. The carbonyls CO₆ and CO₃ (Fig. 6b)
482 were found to be the most frequent recognition sites in the simulations of halobipyridines exhibiting
483 high experimental selectivity. In several cases, the results of the statistical evaluation of the observed
484 contacts in the course of the four MDs were consistent with the experimental EEOs. The EEOs assigned
485 on a model based exclusively on XB interactions were in agreement with the experimental EEO in 18
486 simulations out of 32, with an overall success rate of 56.2%. It is worth noting that the rate increases to
487 75% considering the CDMPC exclusively, whereas it decreases to 37.5% for ADMPC. This evidence
488 could be related to the fact that on ADMPC other entropy-driven forces had been found to control
489 enantioselectivity along XB [109]. Consequently, it was likely that an exclusive XB model does not
490 adequately describe XB-driven enantioseparations on the amylose-based CSP.

491 MD simulations were also performed to model the interaction modes of compound **29** (Fig. 7a) with
492 the CDMPC, hypothesizing the occurrence of a chalcogen bond between the electrophilic sulfur on **29**
493 and the CSP carbonyls as acceptors (Fig. 7) [111].



495 **Figure 7.** Structure of compound **29** and comparison of the occupancy graphs of the MD simulations of CDMPC-**29**
496 complexes over 10 ns: a) CDMPC/(*P*)-**29** (MAD) vs b) CDMPC/(*P*)-**29** (without MAD).

497 A massless dummy atom (MAD) connected to sulfur was introduced manually, by using distance (1.6
498 Å) and charge (0.2 units of positive charge) fixed arbitrarily. In all simulations performed by using the
499 MAD correction, contacts between sulfur and the carbonyl groups of the carbamate moieties of the CSP
500 were observed. The occupancy analysis was also performed in order to evaluate which regions of space
501 were highly populated by the analyte over 10 ns of simulation time. Interestingly, by using the MAD,
502 the first eluted enantiomer (*M*)-**29** showed occupancy volumes in the outer region of the CSP, whereas
503 for the second eluted enantiomer (*P*)-**29** occupancy volumes were also generated in the inner regions of
504 the polymer (Fig. 7b). On the contrary, the occupancy volumes for the enantiomer (*P*)-**29** were shown to
505 move toward the outer regions of the polymer when the MAD correction was not applied (Fig. 7c).

506 **8 Concluding remarks**

507 Nowadays, the use of MM methods suitable for studying large molecular systems and the ongoing
508 improvement in both software and hardware tools are making molecular modelling more and more
509 faithful to simulate enantiomer distinction. A multidisciplinary approach based on the use of orthogonal
510 techniques, involving also molecular modelling, usually enables researchers to obtain reliable
511 mechanistic information. In addition, there is a tendency to develop computational software and
512 platform increasingly friendly. On the one hand, some key steps appear to be crucial in modelling the
513 spatial proximity of selector and selectand in solvated environment: i) choice of force fields suitable for
514 both selectors and selectands, in particular when high-molecular weight selectors have to be treated; ii)
515 the theoretical environment needs to be consistent with the experimental conditions, for example in
516 terms of solvent composition; iii) the design of both selector and selectand involved in the simulation
517 should be made taking into account the responses expected by the simulations. Indeed, the comparison
518 of the computational responses for structurally related series of analytes and selectors can provide useful
519 information about the impact on recognition of focused frameworks and structural variations; iv) all
520 choices should always emerge from a balanced compromise between the need to obtain theoretical

521 results as reliable as possible and approximations, which are dependent on computational time and
522 performances, and complexity of the modelled chromatographic system.

523 In this context, docking and MD strategies provide several types of information on chiral recognition:

524 i) molecular level justifications of observed chromatographic behaviours, in particular the experimental
525 EEO; ii) visualization and binding energies of selector-selectand associations; iii) definition of type,
526 topology, and geometrical parameters (distance, angle) of noncovalent interactions underlying the
527 complexes. Importantly, in our recent studies, MD simulations contributed to develop a recognition
528 model for the emergent σ -hole bond-driven enantioseparations.

529 Finally, it is worth noting that knowledge of chiral recognition mechanisms allows researchers to
530 improve selector-selectand system performance with the aim of optimizing selectivity [130], all the
531 while paving the way to emerging fields of supramolecular separation science like chiral sensing [131]
532 and other chiral surface related recognition phenomena [132].

533 *The authors declared no conflict of interest.*

534 **9 References**

- 535 [1] Lämmerhofer, M., *J. Chromatogr. A* 2010, *1217*, 814-856.
- 536 [2] Chankvetadze, B., *J. Chromatogr. A* 2018, *1567*, 2-25.
- 537 [3] Krait, S., Salgado, A., Chankvetadze, B., Gago, F., Scriba, G. K. E., *J. Chromatogr. A* 2018,
538 *1567*, 198-210.
- 539 [4] Chankvetadze, B., *J. Chromatogr. A* 2012, *1269*, 26-51.
- 540 [5] Li, X., Chang, C., Wang, X., Bai, Y., Liu, H., *Electrophoresis* 2014, *35*, 2733–2743.
- 541 [6] Scriba, G. K. E., *J. Chromatogr. A* 2016, *1467*, 56-78.
- 542 [7] Speybrouck, D., Lipka, E., *J. Chromatogr. A* 2016, *1467*, 33-55.
- 543 [8] Peluso, P., Mamane, V., Aubert, E., Cossu, S., *Electrophoresis* 2017, *38*, 1830-1850.
- 544 [9] Fanali, S., *Electrophoresis* 2017, *38*, 1822-1829.
- 545 [10] Peluso, P., Mamane, V., Aubert, Cossu, S., *J. Chromatogr. A* 2014, *1345*, 182-192.

- 546 [11] Peluso, P., Mamane, V., Aubert, E., Dessì, A., Dallochio, R., Dore, A., Pale, P., Cossu, S., *J.*
547 *Chromatogr. A* 2016, *1467*, 228-238.
- 548 [12] Vanommeslaeghe, K., Guvench, O., MacKerell Jr., A. D., *Curr. Pharm. Des.* 2014, *20*, 3281-
549 3292.
- 550 [13] Adcock, S. A., McCammon, J. A., *Chem. Rev.* 2006, *106*, 1589-1615.
- 551 [14] Lipkowitz, K. B., *J. Chromatogr. A* 2001, *906*, 417-442.
- 552 [15] Lindsey, R. K., Rafferty, J. L., Eggimann, B. L., Siepmann, J. I., Schure, M. R., *J. Chromatogr.*
553 *A* 2013, *1287*, 60-82.
- 554 [16] Scriba, G. K. E., *Chromatographia* 2012, *75*, 815-838.
- 555 [17] Stavrou, I. J., Agathokleous, E. A., Kapnissi-Christodoulo, C. P., *Electrophoresis* 2017, *38*,
556 786-819.
- 557 [18] Sardella, R., Ianni, F., Macchiarulo, A., Pucciarini, L., Carotti, A., Natalini, B., *Mini-Rev. Med.*
558 *Chem.* 2018, *18*, 88-97.
- 559 [19] Lipkowitz, K. B., *J. Chromatogr. A* 1995, *694*, 15-37.
- 560 [20] Lipkowitz, K. B., *Acc. Chem. Res.* 2000, *33*, 555-562.
- 561 [21] Felinger, A., *J. Chromatogr. A* 2008, *1184*, 20-41.
- 562 [22] Karthikeyan, M., Vyas, R., *Practical Chemoinformatics*, Springer India 2014, pp. 195-197.
- 563 [23] Morris, G. M., Goodsell, D. S., Halliday, R. S., Huey, R., Hart, W. E., Belew, R. K., Olson, A.
564 J., *J. Comput. Chem.* 1998, *19*, 1639-1662.
- 565 [24] Morris, G. M., Huey, R., Lindstrom, W., Sanner, M. F., Belew, R. K., Goodsell, D. S., Olson,
566 A. J., *J. Comput. Chem.* 2009, *30*, 2785-2791.
- 567 [25] Ravichandran, S., Collins, J. R., Singh, N., Wainer, I. W., *J. Chromatogr. A* 2012, *1269*, 218-
568 225.
- 569 [26] Tsai, C. S., *An Introduction to Computational Biochemistry*, Wiley-Liss, Inc., New York 2002,
570 pp. 292-295 (MDs) and pp. 320-322 (docking).

- 571 [27] Giddings, J. C., Eyring, H., *J. Phys. Chem.* 1955, *59*, 416-421.
- 572 [28] Young, D. C., *Computational Drug Design*, John Wiley & Sons, Inc. Hoboken, New Jersey
573 2009, p. 294.
- 574 [29] Case, J. T. B. D. A., Betz, R. M., Cerutti, D. S., Cheatham III, T. E., Darden, T. A., Duke, R.
575 E., Giese, T. J., Gohlke, H., Goetz, A.W., Homeyer, N., Izadi, S., Janowski, P., Kaus, J.,
576 Kovalenko, A., Lee, T. S., LeGrand, S., Li, P., Luchko, T., Luo, R., Madej, B., Merz, K. M.,
577 Monard, G., Needham, P., Nguyen, H., Nguyen, H. T., Omelyan, I., Onufriev, A., Roe, D. R.,
578 Roitberg, A., Salomon-Ferrer, R., Simmerling, C. L., Smith, W., Swails, J., Walker, R. C.,
579 Wang, J., Wolf, R. M., Wu, X., York, D. M., Kollman, P. A., AMBER 2015, University of
580 California, San Francisco, 2015.
- 581 [30] Brooks, B. R., Bruccoleri, R. E., Olafson, B. D., States, D. J., Swaminathan, S., Karplus, M., *J.*
582 *Comput. Chem.* 1983, *4*, 187-217.
- 583 [31] Patodia, S., Bagaria, A., Chopra, D., *J. Phys. Chem. Biophys.* 2014, *4*, 1-4.
- 584 [32] Anandakrishnan, R., Drozdetski, A., Walker, R. C., Onufriev, A. V., *Biophys. J.* 2015, *108*,
585 1153-1164.
- 586 [33] Alonso, H., Bliznyuk, A. A., Gready, J. E., *Med. Res. Rev.* 2006, *26*, 531-568.
- 587 [34] Hospital, A., Goñi, J. R., Orozco, M., Gelpí, J. L., *Adv. App. Bioinf. Chem.* 2015, *8*, 37-47.
- 588 [35] Fernandes, C., Phyo, Y. Z., Silva, A. S., Tiritan, M. E., Kijjoa, A., Pinto, M. M. M., *Sep. Purif.*
589 *Rev.* 2018, *47*, 89-123.
- 590 [36] Zhao, C. F., Cann, N. M., *J. Chromatogr. A* 2006, *1131*, 110-129.
- 591 [37] Zhao, C. F., Cann, N. M., *Anal. Chem.* 2008, *80*, 2426-2438.
- 592 [38] Hall, K., Ashtari, M., Cann, N. M., *J. Chem. Phys.* 2012, *136*, 114705, doi: 10.1063/1.3693516.
- 593 [39] Alcaro, S., Gasparrini, F., Incani, O., Mecucci, S., Misiti, D., Pierini, M., Villani, C., *J. Comput.*
594 *Chem.* 2000, *21*, 515-530.

- 595 [40] Alcaro, S., Gasparrini, F., Incani, O., Caglioti, L., Pierini, M., Villani, C., *J. Comput. Chem.*
596 2007, 28, 1119-1128.
- 597 [41] Ashtari, M., Cann, N. M., *J. Chromatogr. A* 2011, 1218, 6331-6347.
- 598 [42] Ashtari, M., Cann, N. M., *J. Chromatogr. A* 2012, 1265, 70-87.
- 599 [43] Ashtari, M., Cann, N. M., *J. Chromatogr. A* 2015, 1409, 89-107.
- 600 [44] Çakmak, R., Ercan, S., Sünkür, M., Yilmaz, H., Topal, G., *Org. Commun.* 2017, 10, 216-227.
- 601 [45] Lämmerhofer, M., *Anal. Bioanal. Chem.* 2014, 406, 6095-6103.
- 602 [46] Lämmerhofer, M., Lindner, W., *J. Chromatogr. A* 1996, 741, 33-48.
- 603 [47] Sardella, R., Carotti, A., Gioiello, A., Lisanti, A., Ianni, F., Lindner, W., Natalini, B., *J.*
604 *Chromatogr. A* 2014, 1339, 96-102.
- 605 [48] Sardella, R., Lisanti, A., Carotti, A., Blasi, P., Lindner, W., Natalini, B., *J. Sep. Sci.* 2014, 37,
606 2696-2703.
- 607 [49] Ianni, F., Carotti, A., Marinozzi, M., Marcelli, G., Di Michele, A., Sardella, R., Lindner, W.,
608 Natalini, B., *Anal. Chim. Acta* 2015, 885, 174-182.
- 609 [50] Grecsó, N., Kohout, M., Carotti, A., Sardella, R., Natalini, B., Fülöp, F., Lindner, W., Péter, A.,
610 Ilisz, I., *J. Pharm. Biomed. Anal.* 2016, 124, 164-173.
- 611 [51] Sardella, R., Macchiarulo, A., Urbinati, F., Ianni, F., Carotti, A., Kohout, M., Lindner, W.,
612 Péter, A., Ilisz, I., *J. Sep. Sci.* 2018, 41, 1199-1207.
- 613 [52] Ianni, F., Pucciarini, L., Carotti, A., Gioiello, A., Galarini, R., Natalini, S., Sardella, R.,
614 Lindner, W., Natalini, B., *J. Chromatogr. A* 2018, 1557, 20-27.
- 615 [53] Guo, Z., Mohanty, U., Noehre, J., Sawyer, T.K., Sherman, W., Krilov, G., *Chem. Biol. Drug*
616 *Des.* 2010, 75, 348-359.
- 617 [54] Okamoto, Y., Yashima, E., *Angew. Chem. Int. Ed.* 1998, 37, 1020-1043.
- 618 [55] Yashima, E., Yamada, M., Kaida, Y., Okamoto, Y., *J. Chromatogr. A* 1995, 694, 347-354.
- 619 [56] Yamamoto, C.; Yashima, E.; Okamoto, Y. *J. Am. Chem. Soc.* 2002, 124, 12583-12589.

- 620 [57] Yamamoto, C., Yashima, E., Okamoto, Y., *Bull. Chem. Soc. Jpn.* 1999, 72, 1815-1825.
- 621 [58] Kasat, R. B., Wang, N. H. L., Franses, E. I., *Biomacromolecules* 2007, 8, 1676-1685.
- 622 [59] Kasat, R. B., Wang, N. H. L., Franses, E. I., *J. Chromatogr. A* 2008, 1190, 110-119.
- 623 [60] Kasat, R. B., Franses, E. I., Wang, N. H. L., *Chirality* 2010, 22, 565-579.
- 624 [61] O'Brien, T., Crocker, L., Thompson, R., Thompson, K., Toma, P. H., Conlon, D. A., Feibush,
625 B., Moeder, C., Bicker, G., Grinberg, N., *Anal. Chem.* 1997, 69, 1999-2007.
- 626 [62] Ma, S., Tsui, H. -W., Spinelli, E., Busacca, C. A., Franses, E. I., Wang, N. H. L., Wu, L., Lee,
627 H., Senanayake, C., Yee, N., Gonella, N., Fandrick, K., Grinberg, N., *J. Chromatogr. A* 2014,
628 1362, 119-128.
- 629 [63] Booth, T. D., Wainer, I. W., *J. Chromatogr. A* 1996, 737, 157-169.
- 630 [64] Ye, Y. K., Bai, S., Vyas, S., Wirth, M. J., *J. Phys. Chem. B* 2007, 111, 1189-1198.
- 631 [65] Li, Y., Liu, D., Wang, P., Zhou, Z., *J. Sep. Sci.* 2010, 33, 3245-3255.
- 632 [66] Kim, B. -H., Lee, S. U., Moon, D. C., *Chirality* 2012, 24, 1037-1046.
- 633 [67] Ortuso, F., Alcaro, S., Menta, S., Fioravanti, R., Cirilli, R., *J. Chromatogr. A* 2014, 1324, 71-
634 77.
- 635 [68] Zhao, L., Xie, J., Guo, F., Liu, K., *Chirality* 2018, 30, 661-669.
- 636 [69] Ali, I., Haque, A., Al-Othman, Z. A., Al-Warthan, A., Asnin, L., *Sci. China Chem.* 2015, 58,
637 519-525.
- 638 [70] Ali, I., Sahoo, D. R., Al-Othman, Z. A., Al-Warthan, A., Asnin, L., Larsson, B., *J. Chromatogr.*
639 *A* 2015, 1406, 201-209.
- 640 [71] Ali, I., Lone, M. N., Suhail, M., Al-Othman, Z. A., Al-Warthan, A., *RSC Adv.* 2016, 6, 14372-
641 14380.
- 642 [72] Zhu, B., Zhao, F., Yu, J., Wang, Z., Song, Y., Li, Q., *New J. Chem.* 2018, 42, 13421-13429.
- 643 [73] Li, M., Zhang, B., Yu, J., Wang, J., Guo, X., *New J. Chem.* 2018, 42, 11724-11731.
- 644 [74] Hu, G., Huang, M., Luo, C., Wang, Q., Zou, J. -W., *J. Mol. Graph. Model.* 2016, 66, 123-132.

- 645 [75] Zhao, B., Oroskar, P. A., Wang, X., House, D., Oroskar, A., Oroskar, A., Jameson, C., Murad,
646 S., *Langmuir* 2017, 33, 11246-11256.
- 647 [76] Rossi, D., Nasti, R., Collina, S., Mazzeo, G., Ghidinelli, S., Longhi, G., Memo, M., Abbate, S.,
648 *J. Pharm. Biomed. Anal.* 2017, 144, 41-51.
- 649 [77] Dou, X., Su, X., Wang, Y., Chen, Y., Shen, W., *Chirality* 2015, 27, 802-808.
- 650 [78] Pisani, L., Rullo, M., Catto, M., de Candia, M., Carrieri, A., Cellamare, S., Altomare, C. D., *J.*
651 *Sep. Sci.* 2018, 41, 1376-1384.
- 652 [79] Gogolashvili, A., Tatumashvili, E., Chankvetadze, L., Sohajda, T., Szemann, J., Salgado, A.,
653 Chankvetadze, B., *Electrophoresis* 2017, 38, 1851-1859.
- 654 [80] Melani, F., Pasquini, B., Caprini, C., Gotti, R., Orlandini, S., Furlanetto, S., *J. Pharm. Biomed.*
655 *Anal.* 2015, 114, 265-271.
- 656 [81] Salgado, A., Chankvetadze, B., *J. Chromatogr. A*, 2016, 1467, 95-144.
- 657 [82] Quevedo, M. A., Zoppi, A., *J. Incl. Phenom. Macrocycl. Chem.* 2018, 90, 1-14.
- 658 [83] Alvira, E., *Tetrahedron: Asymmetry* 2013, 24, 1198-1206.
- 659 [84] Alvira, E., *Tetrahedron: Asymmetry* 2015, 26, 853-860.
- 660 [85] Alvira, E., *Chemical Physics Letters* 2017, 679, 31-37.
- 661 [86] Li, X., Yao, X., Xiao, Y., Wang, Y., *Anal. Chim. Acta* 2017, 990, 174-184.
- 662 [87] Matencio, A., Bermejo-Gimeno, M. J., García-Carmona, F., López-Nicolás, J. M., *Phytochem.*
663 *Anal.* 2017, 28, 151-158.
- 664 [88] Suliman, F. O., Elbashir, A. A., Schmitz, O. J., *J. Incl. Phenom. Macrocycl. Chem.* 2015, 83,
665 119-129.
- 666 [89] Arsad, S. R., Maarof, H., Ibrahim, W. A. W., Aboul-Enein, H. Y., *Chirality* 2016, 28, 209-214.
- 667 [90] Yang, X., Du, Y., Feng, Z., Liu, Z., Li, J., *J. Chromatogr. A* 2018, 1559, 170-177.
- 668 [91] Li, J., Yu, T., Xu, G., Du, Y., Liu, Z., Feng, Z., Yang, X., Xi, Y., Liu, J., *J. Chromatogr. A*
669 2018, 1559, 178-185.

- 670 [92] Yang, X., Yan, Z., Yu, T., Du, Y., Chen, J., Liu, Z., Xi, Y., *Anal. Bioanal. Chem.* 2018, *410*,
671 5889-5898.
- 672 [93] Li, L., Li, X., Luo, Q., You, T., *Talanta* 2015, *142*, 28-34.
- 673 [94] Pasquini, B., Melani, F., Caprini, C., Del Bubba, M., Pinzauti, S., Orlandini, S., Furlanetto, S.,
674 *J. Pharm. Biomed. Anal.* 2017, *144*, 220-229.
- 675 [95] Salgado, A., Tatumashvili, E., Gogolashvili, A., Chankvetadze, B., Gago, F., *Phys. Chem.*
676 *Chem. Phys.* 2017, *19*, 27935-27939.
- 677 [96] Sun, P., Wang, C., Breitbach, Z. S., Zhang, Y., Armstrong, D. W., *Anal. Chem.* 2009, *81*,
678 10215-10226.
- 679 [97] Wang, L., Li, C., Yin, Q., Zeng, S., Sun, C., Pan, Y., Armstrong, D. W., *Tetrahedron* 2015, *71*,
680 3447-3452.
- 681 [98] Phyto, Y. Z., Cravo, S., Palmeira, A., Tiritan, M. E., Kijjoa, A., Pinto, M. M. M., Fernandez, C.,
682 *Molecules* 2018, *23*, 142, doi: 10.3390/molecules23010142.
- 683 [99] Ali, I., Suhail, M., Asnin, L., *Chirality* 2018, doi: 10.1002/chir.23024.
- 684 [100] Sobiech, M., Żołek, T., Luliński, P., Maciejewska, D., *Talanta* 2016, *146*, 556-567.
- 685 [101] Lee, O. -S., *J. Comput. Sci.* 2016, *15*, 60-64.
- 686 [102] Morris, K. F., Billiot, E. J., Billiot, F. H., Hoffman, C. B., Gladis, A. A., Lipkowitz, K. B.,
687 Southerland, W. M., Fang, Y., *Chem. Physics* 2015, *457*, 133-146.
- 688 [103] Morris, K. F., Billiot, E. J., Billiot, F. H., Ingle, J. A., Zack, S. R., Krause, K. B., Lipkowitz, K.
689 B., Southerland, W. M., Fang, Y., *J. Dispersion Sci. Tech.* 2018, *39*, 45-54.
- 690 [104] Feder-Kubis, J., Flieger, J., Tatarczak-Michalewska, M., Płazińska, A., Madejska, A., Swatko-
691 Ossord, M., *RSC Adv.* 2017, *7*, 32344–32356.
- 692 [105] Peluso, P., Mamane, V., Aubert, E., Cossu, S., *J. Chromatogr. A* 2012, *1251*, 91–100.
- 693 [106] Peluso, P., Mamane, V., Aubert, E., Cossu, S., *J. Sep. Sci.* 2013, *36*, 2993–3003.
- 694 [107] Peluso, P., Mamane, V., Aubert, E., Cossu, S., *J. Sep. Sci.* 2014, *37*, 2481–2489.

- 695 [108] Peluso, P., Mamane, V., Cossu, S., *Chirality* 2015, 27, 667–684.
- 696 [109] Peluso, P., Mamane, V., Dallochio, R., Dessì, A., Villano, R., Sanna, D., Aubert, E., Pale, P.,
697 Cossu, S., *J. Sep. Sci.* 2018, 41, 1247–1256.
- 698 [110] Dallochio, R., Dessì, A., Solinas, M., Arras, A., Cossu, S., Aubert, E., Mamane, V., Peluso, P.,
699 *J. Chromatogr. A* 2018, 1563, 71–81.
- 700 [111] Peluso, P., Gatti, C., Dessì, A., Dallochio, R., Weiss, R., Aubert, E., Pale, P., Cossu, S.,
701 Mamane, V., *J. Chromatogr. A* 2018, 1567, 119–129.
- 702 [112] Desiraju, G. R., Ho, P. S., Kloo, L., Legon, A. C., Marquardt, R., Metrangolo, P., Politzer, P.,
703 Resnati, G., Rissanen, K., *Pure Appl. Chem.* 2013, 85, 1711–1713.
- 704 [113] Cavallo, G., Metrangolo, P., Milani, R., Pilati, T., Priimagi, A., Resnati, G., Terraneo, G.,
705 *Chem. Rev.* 2016, 116, 2478–2601.
- 706 [114] Mahmudov, K. T., Kamran, T., Kopylovich, M. N., Guedes da Silva, M. F. C., Pombeiro, A. J.
707 L., *Dalton Trans.* 2017, 46, 10121–10138.
- 708 [115] Politzer, P., Murray, J. S., Clark T., *Phys. Chem. Chem. Phys.* 2013, 15, 11178–11588.
- 709 [116] Kolář, M. H., Hobza, P., *Chem. Rev.* 2016, 116, 5155–5187.
- 710 [117] Ibrahim, M. A. A., *J. Comput. Chem.* 2011, 32, 2564–2574.
- 711 [118] Ibrahim, M. A. A., *J. Mol. Model.* 2012, 18, 4625–4638.
- 712 [119] Rendine, S., Pieraccini, S., Forni, A., Sironi, M., *Phys. Chem. Chem. Phys.* 2011, 13, 19508–
713 19516.
- 714 [120] Franchini, D., Dapiaggi, F., Pieraccini, S., Forni, A., Sironi, M., *Chem. Phys. Lett.* 2018, 712,
715 89–94.
- 716 [121] Kolář, M., Pavel Hobza, P., *J. Chem. Theory Comput.* 2012, 8, 1325–1333.
- 717 [122] Kolář, M., Hobza, P., Bronowska, K., *Chem. Commun.* 2013, 49, 981–983.
- 718 [123] Jorgensen, W. L., Schyman, P., *J. Chem. Theory Comput.* 2012, 8, 3895–3901.

- 719 [124] Yan, X. C., Robertson, M. J., Tirado-Rives, J., Jorgensen, W. L., *J. Phys. Chem. B* 2017, *121*,
720 6626–6636.
- 721 [125] Zhou, Y., Wang, Y., Li, P., Huang, X.-P., Qi, X., Du, Y., Huang, N., *ACS Chem. Med. Lett.*
722 2018, *9*, 1019–1024.
- 723 [126] Lim, J. Y. C., Marques, I., Thompson, A. L., Christensen, K. E., Félix, V., Beer, P. D., *J. Am.*
724 *Chem. Soc.* 2017, *139*, 3122–3133.
- 725 [127] Lim, J. Y. C., Marques, I., Félix, V., Beer, P. D., *Angew. Chem. Int. Ed.* 2018, *57*, 584–588.
- 726 [128] Gutiérrez, I. S., Lin, F.-Y., Vanommeslaeghe, K., Lemkul, J. A., Armacost, K. A., Brooks III,
727 C. L., MacKerell, A. D., *Biorg. Med. Chem.* 2016, *24*, 4812–4825.
- 728 [129] Nunes, R., Vila-Viçosa, D., Machuqueiro, M., Costa, P. J., *J. Chem. Theory Comput.* 2018, *14*,
729 5393–5392
- 730 [130] Schurig, V., *Molecules* 2016, *21*, 1535; doi:10.3390/molecules21111535.
- 731 [131] Manoli, K., Magliulo, M., Torsi, L., in: Schurig, V. (Ed.), *Differentiation of Enantiomers II*,
732 Springer International Publishing, Switzerland 2013, pp. 133-176.
- 733 [132] Lang, J. C., Armstrong, D. W., *Curr. Opin. Colloid Interface Sci.* 2017, *32*, 94-107.
734
735